Available online at www.sciencedirect.com

ScienceDirect

journal homepage: www.elsevier.com/locate/he

CFD simulation of methane steam reforming in a membrane reactor: Performance characteristics over range of operating window

Mukesh Upadhyay [a], *Hyunjun Lee* [a], *Ayeon Kim* [a], *Sang-hun Lee* [b,**], *Hankwon Lim* [a,c,*]

[a] *School of Energy and Chemical Engineering, Ulsan National Institute of Science and Technology (UNIST), 50 UNIST-gil, Eonyang-eup, Ulju-gun, Ulsan, 44919, Republic of Korea*

[b] *Department of Environmental Science, Keimyung University, Dalgubeol-daero 1095, Daegu, 42601, Republic of Korea*

[c] *Department of Energy Engineering, Ulsan National Institute of Science and Technology (UNIST), 50 UNIST-gil, Eonyang-eup, Ulju-gun, Ulsan, 44919, Republic of Korea*

HIGHLIGHTS

- 3D CFD analysis of methane steam reforming in a membrane reactor.
- Xu forment based kinetic model and Sieverts' law-based permeation model were coupled.
- The CFD model evaluates the temperature, GHSV, S/C ratio and sweep gas flow pattern.
- Key performance phenomena were identified, and optimum conditions were suggested.

GRAPHICAL ABSTRACT

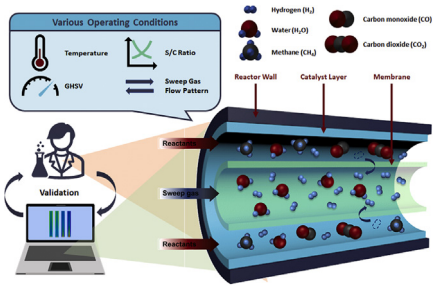

ARTICLE INFO

Article history:
Received 31 January 2021
Received in revised form
3 June 2021
Accepted 23 June 2021
Available online 15 July 2021

Keywords:
Membrane reactor
Computational fluid dynamics
Palladium (pd) membrane

ABSTRACT

Methane steam reforming is the most widely used pathway for hydrogen production. In this context, the use of a fixed bed catalytic reactor with a hydrogen-selective membrane is one of the most promising technologies to produce high purity hydrogen gas. In this work, the membrane reactor three-dimensional computational fluid dynamic (CFD) model was developed to investigate the performance. In this model, methane steam reforming global kinetic model has been coupled with the CFD model using User-Defined Function (UDF). Whereas, hydrogen permeation across the membrane is implemented by introducing source and sink formulation. The CFD simulation results were compared to the experimental data, where the developed model successfully captured the experimentally observed trends. We studied the influence of the various operating parameters, as temperature, steam to carbon ratio, sweep gas flow configuration and space velocity on the

* *Corresponding author*. School of Energy and Chemical Engineering, Ulsan National Institute of Science and Technology (UNIST), 50 UNIST-gil, Eonyang-eup, Ulju-gun, Ulsan 44919, Republic of Korea.
** *Corresponding author*.
E-mail addresses: shlee73@kmu.ac.kr (S.-h. Lee), hklim@unist.ac.kr (H. Lim).
https://doi.org/10.1016/j.ijhydene.2021.06.178

Methane steam reforming
Hydrogen separation

overall performance. The main observation and attained optimal operation windows from the study was discussed to provide insight into the factors affecting the overall performance.

Introduction

The industrial scale methane and other hydrocarbon fuel conversion to hydrogen (H_2) is carried out by three main methods: steam reforming, partial oxidation, and auto-thermal reforming [1]. Among them methane steam reforming (MSR) has been accounting for approximately 48% of global H_2 production [2–5]. Hydrogen-selective membranes have been employed in conventional packed bed reactors (PBR) and offer several advantages in terms of cost effectiveness and process efficiency [6–8]. The advantages include the increase in H_2 production rate compared to that of a packed bed reactor at the same temperature. Moreover, membrane reactor (MR) can operate at milder conditions than conventional PBR. Another advantage of this hydrogen-selective membrane reactor is the conservation of additional H_2 purification equipment cost. All these above-mentioned advantages stem due to Le Chatelier's principle.

The development of inorganic membranes has received attention because of their potential application for medium-high temperature operations. Particularly for the application of hydrogen gas separation several membranes have already been developed with various raw materials such as dense polymer, dense ceramic, dense metallic, porous carbon, mixed matrix membrane, etc. [9–13]. Among those, dense metallic-based membranes, especially Palladium (Pd) membranes, provide higher hydrogen perm-selectivity than those with other materials. Further, Palladium (Pd) membranes do not form an oxide layer unlike other dense membranes such as tantalum (Ta), niobium (Nb), and vanadium (V). Addition of alloying elements for example copper (Cu), yttrium (Y) and silver (Ag) help to improves H_2 permeability and mechanical durability with no effect on selectivity. In literature, hollow fiber, flat-sheet, and tubular type metallic membranes were used for methane reforming process [6,14,15]. In membrane reactor, a pressure gradient is driving force for the hydrogen permeation. Essentially, high-pressure feed gas mixture is applied to the retentate side while maintaining low pressure on the permeate side. Higher hydrogen partial pressure seeds the permeation from high to low pressure.

Several researchers have studied the hydrogen separation utilizing a Pd-based membrane. Iulianelli et al. [16] perform the comparative experiment for MSR with and without Pd-MR at 450 °C and low pressures (1–3 bar). Observe methane conversion obtained in the PBR is 6% with respect to 50% obtained with the MR. Kim et al. [17] carried out MSR reaction at gas hourly space velocity (GHSV) = 1700 h^{-1}, 773 K and steam to carbon ratio (S/C) = 3.0, for ~145 h in tubular Pd-based composite membrane reactor with a commercial Ru/Al_2O_3 catalyst. Methane conversion increased at a higher transmembrane pressure difference, and reached 79.5% at a transmembrane pressure difference of 507 kPa. Nayebossadri et al. [18] studied hydrogen separation from blended natural gas and hydrogen using commercially available Pd, $PdCu_{53}$, and $PdAg_{24}$ membranes. Separation capability was investigated under different hydrogen concentration, partial pressure, and temperature. Also, a possible interaction between gas impurity and membranes was investigated. Among these membranes, $PdAg_{24}$ effectively separated hydrogen concentrations as low as 15%. The use of Pd-based membranes requires large pressure gradient across the membrane surface and high temperatures (>350 °C) [19]. On the other hand, H_2 rich gases containing CO affect H_2 permeation performance [20]. All these factors make required to explore the qualitative behavior under different operating conditions.

As mentioned above, the experimental observations confirmed the advantageous feature of a membrane reactor including Pd-membranes. Currently, a variety of modeling tools have been utilized to predict reactor performances and facilitate the optimization of membrane reactors [21]. For example, modeling based on a one-dimensional (1-D) plug flow reactor is probably the simplest approach, but this method does not take into account comprehensive information pertaining to temperature, concentration, or velocity profiles [22,23]. Thus, more advanced simulation tools such as a multi-dimensional computational fluid dynamics (CFD) model should be provided to predict further realistic temporal and spatial distributions within membrane reactors. Benguerba et al. [24,25] developed a CFD model to study hydrogen separation through nickel/α-alumina membrane. At low pressure, the performance of porous nickel membrane competed with the Pd–Ag membrane, but at higher pressure, nickel membrane selectivity weaken. Ghohe and Hormozi [26] numerically investigated the influence of geometrical shape on H_2 separation over Pd-membrane using two-dimensional CFD model. Their study shows a higher average flux for conical shape compared to the cylindrical shape. Chen et al. [27] optimized multiple Pd membrane tube distribution to maximize the separation of CO_2 and H_2. They showed that increase in the number of tubes raises the optimization efficiency. Optimized configuration at Re = 10 the CO_2 enrichment intensified by up to 7%, while hydrogen recovery up to 12.2%. Also, researchers paid attention to model chemical kinetics and separation phenomena in the single unit reactor [28]. Wei-Hsin Chen et al. [29] model hydrogen flux and concentration polarization in the palladium (Pd) membrane. In the membrane, source-sink terms following Sieverts' law were used in numerical study. Their numerical result show, higher hydrogen separation with counter-current flow compared to co-current flow configuration. Further, an increase in reactant feed rate with sweep gas influence the hydrogen permeation by increasing

the concentration polarization. Coroneo et al. [30] performed a CFD simulation for three different kinds of inorganic membrane modules. Their model introduced sink and source terms on the membrane boundary cells and shows good prediction against experimental data. Said et al. [31,32] simulated a molten salt-heated membrane reformer integrated into a parabolic trough solar facility. A 2D CFD model was developed to investigate and optimize the performance of a catalyst-assisted membrane-based reformer for hydrogen. Their operating temperature range was found to be suitable to make the reformer as the receiver of a parabolic trough solar collector. Sanusi et al. [33] simulated a membrane-based reformer–combustor reactor using CFD. Reforming, sweep, and combustion zone were simulated with 2-D axisymmetric domain. Firstly, methane steam reforming model was validated, and further membrane rector was verified for different temperature. Their model study was firstly validated for methane steam reforming model then membrane rector was further validated for different temperature sets. Xuan et al. [34] performed a numerical simulation of a microchannel reformer with a catalytic-supported membrane. In their study, a two-dimensional CFD model combined with chemical kinetics was developed with a key objective focusing on the modeling of local heat and mass transfer phenomena rather than whole system performance. Tahmasbi et al. [35] presented 2D axisymmetric CFD model of the silica membrane for H_2 separation. On the tube zone species transfer was defined by source terms, whereas on the shell side transport of species was specified.

In spite of the many research accomplishments so far, all the above-mentioned simulation studies were mostly limited to the utilization of simplified 2D geometry or neglecting the steam reforming reaction in a reaction zone. Also, integration of the reaction kinetics and hydrogen separation were not considered within 3D geometry in previous models. In reality, it is desirable that both phenomena take place simultaneously should be incorporated in a multi-dimensional model. Furthermore, during long periods of operation, Pd-membrane permeance decline due CO adsorption on the membrane surface. Therefore, the present study primarily aimed to scan the membrane reactor performances over a wide range of space velocities, sweep gas flow reaction temperature including industrially relevant values. The outcomes of the CFD analysis are expected to be helpful for future design and optimization of the membrane modules for hydrogen separation.

System description and operating condition

The membrane reactor geometry is created based on the experimental setup of Kim et al. [36]. Fig. 1 describes the three-dimensional membrane reactor geometry used in the simulation. The membrane reactor is composed of two domains: (a) reforming section (retentate domain) and (b) permeate domain separated by membrane layer. The computation domain has a length of 300 mm and a height of 25.4 mm. The membrane reactor was packed with commercial Ni/Al_2O_3 catalyst and Pd–Ru membrane. In the retentate zone reforming reaction takes place, producing H_2, CO_2, and

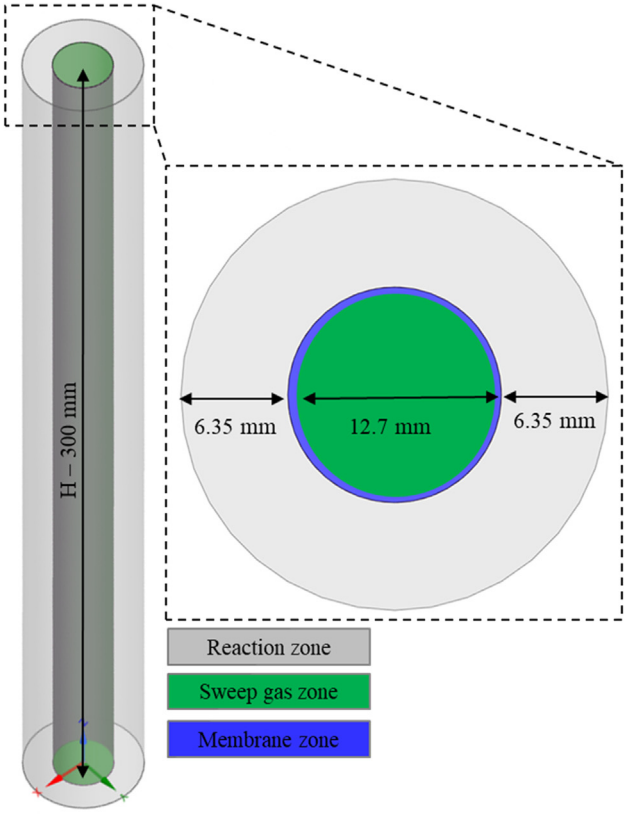

Fig. 1 – 3D membrane reactor computational domain.

CO species and leaves it from the outlet. As the gas species pass over membrane layer hydrogen is instantaneously permeated through the membrane to the permeate domain. In this work, we conceptually consider a permeate domain sweep gas from the bottom and top. The permeated hydrogen leaves the computation domain along with the sweeping gas from the top side of the permeation domain (permeate-outlet). In this work, both the retentate and permeate domain were included in the simulation. Other information on the simulation, such as the reactor geometry, and operating conditions are summarized in Table 1.

Mathematical model

To accurately account the conversion of reactants (steam and methane) into products (hydrogen fuel) under different conditions, researcher coupled the reaction kinetics model with reactor-scale CFD modeling. Catalyst specific detail transport and reaction phenomena kinetic model incorporation is beyond the scope of this study. Therefore, catalyst bed was numerically simulated as porous media with volumetric species transport model. In the present study, widely-accepted simplified global kinetics expressions presented by Xu and Froment [37] are adopted. Tables 2 and 3 summarized the reaction rates with their corresponding kinetic, equilibrium, and adsorption constants. Apart from that, intraparticle diffusion limitations inside catalyst particles were incorporated by effectiveness factors for the reforming reactions [38,39]. For

Table 1 – System geometry and operating conditions.

Description	Value
Temperature, K	673–1273
Retentate pressure, kPa	200, 250
Permeate pressure, kPa	100
Gas hourly space velocity, h^{-1}	837–10000
CH_4: H_2O	1:3
Length, mm	300
Membrane diameter, mm	12.7
Reactor diameter, mm	25.4

the reforming reactions, optimal effectiveness factors value were used.

For the MSR, a commercial spherical Ni/Al_2O_3 (diameter of 1.5 mm) catalyst was used in this study. For Ni/Al_2O_3 catalyst thermal conductivity of 33 W/m/K was used by Lao et al. [40]. For determining the composition, the mixture, mixing-law based on the species mass fraction was used. For calculating the density of mixture, volume-weighted-mixing-law was employed. The viscosity and thermal conductivity were estimated using the ideal-gas mixing law (or mass-weighted mixing law). In the present work, each gas component specific heat capacity (c_p) were determined by a fourth-order polynomial and thermal conductivity (λ_i) was estimated by the kinetic theory [41]. Whereas, the power law expression was used to estimate viscosity of each species.

To estimate the hydrogen permeation rate across the membrane, Sieverts' law-based equation has been widely accepted [42]. In the present numerical work, pair of source and sink terms were implemented in the species transport equation. The overall permeation was calculated by multiplying Sievert's law with a parameter A_c/V_c, where A_c is cell area and V_c is the cell volume, as shown by eq. (4)

$$\phi = \beta . M_{w,H_2} . \frac{A_c}{V_c} . \frac{P_e}{l} . exp\left(-\frac{E_a}{RT}\right)\left(P_{r,H_2}^{0.5} - P_{p,H_2}^{0.5}\right) \quad (4)$$

Results and discussion

Mesh sensitivity analysis

To determine the optimal number of grid cells to achieve both model accuracy and efficiency in simulation, various sets of the cell numbers were applied in a preliminary model test. ANSYS meshing tool was used to discretized the 3D domain into hexahedral grid. Four different grid cell sizes of 2, 1, 0.75, and 0.5 mm were used, for which about 20400, 156300, 362400, and 1253400 number of grid were constructed respectively in order to investigate the effect of grid size (see Fig. 2). Methane conversion was selected as the judging variable to determine whether the model solution needs further refinement. As shown in Fig. 3, a higher methane conversion value was obtained with very course grid, but methane conversion value decreased and finally showed similar conversion for the grid containing up to 156300 mesh numbers. Thus, the grid was not refined further to save the computational time.

Table 3 – The MSR reaction constants.

Kinetic constant coefficients:	$k_1 = 4.22 \times 10^{15} exp\left(-\frac{240,100}{RT}\right)$
	$k_2 = 1.96 \times 10^{6} exp\left(-\frac{67,130}{RT}\right)$
	$k_3 = 1.02 \times 10^{15} exp\left(-\frac{243,900}{RT}\right)$
Equilibrium constants:	$K_{e1} = 1.198 \times 10^{13} exp\left(-\frac{26,830}{RT}\right)$
	$K_{e2} = 1.767 \times 10^{-2} exp\left(\frac{4,400}{RT}\right)$
	$K_{e3} = 2.117 \times 10^{11} exp\left(-\frac{22,430}{RT}\right)$
Adsorption constants:	$K_{CH_4} = 6.65 \times 10^{-4} exp\left(\frac{38,280}{RT}\right)$
	$K_{H_2O} = 1.77 \times 10^{5} exp\left(-\frac{88,680}{RT}\right)$
	$K_{H_2} = 6.12 \times 10^{-9} exp\left(\frac{82,900}{RT}\right)$
	$K_{CO} = 8.23 \times 10^{-5} exp\left(\frac{70,650}{RT}\right)$

Membrane reactor model validation

Before investigating the key operating parameter, the developed MSR kinetic model was verified by operating the retentate domain identical to temperature, pressure, and space velocity of Xu and Froment [37]. The operation condition includes the reaction temperature of 848 K at the pressure of 10 bar with a steam-to-methane (S/C) ratio equal to 3. As a result of the validity test, Fig. 4 (a) depicts the simulated data, compared with their corresponding experimental methane conversion data reported by Xu and Froment [37].

Further, the developed Sieverts' law-based hydrogen permeation model was verified against the experimental data

Table 2 – Methane steam reforming (MSR) reaction rates.

Steam reforming reaction (SR): $CH_4 + H_2O \Rightarrow 3H_2 + CO$	$r_1 = \frac{k_1 (P_{CH_4} P_{H_2O} - P_{H_2}^3 P_{CO} K_{e_1}^{-1})}{P_{H_2}^{2.5} DEN^2}$
Water gas shift reaction (WGSR): $CO + H_2O \Rightarrow H_2 + CO_2$	$r_2 = \frac{k_2 (P_{CO} P_{H_2O} - P_{H_2} P_{CO_2} K_{e_2}^{-1})}{P_{H_2} DEN^2}$
Direct steam reforming reaction (DSR): $CH_4 + 2H_2O \Rightarrow 4H_2 + CO_2$	$r_3 = \frac{k_3 (P_{CH_4} P_{H_2O}^2 - P_{H_2}^4 P_{CO_2} K_{e_3}^{-1})}{P_{H_2}^{3.5} DEN^2}$
	$DEN = 1 + K_{CO} P_{CO} + K_{H_2} P_{H_2} + K_{CH_4} P_{CH_4} + K_{H_2O} \left(\frac{P_{H_2O}}{P_{H_2}}\right)$

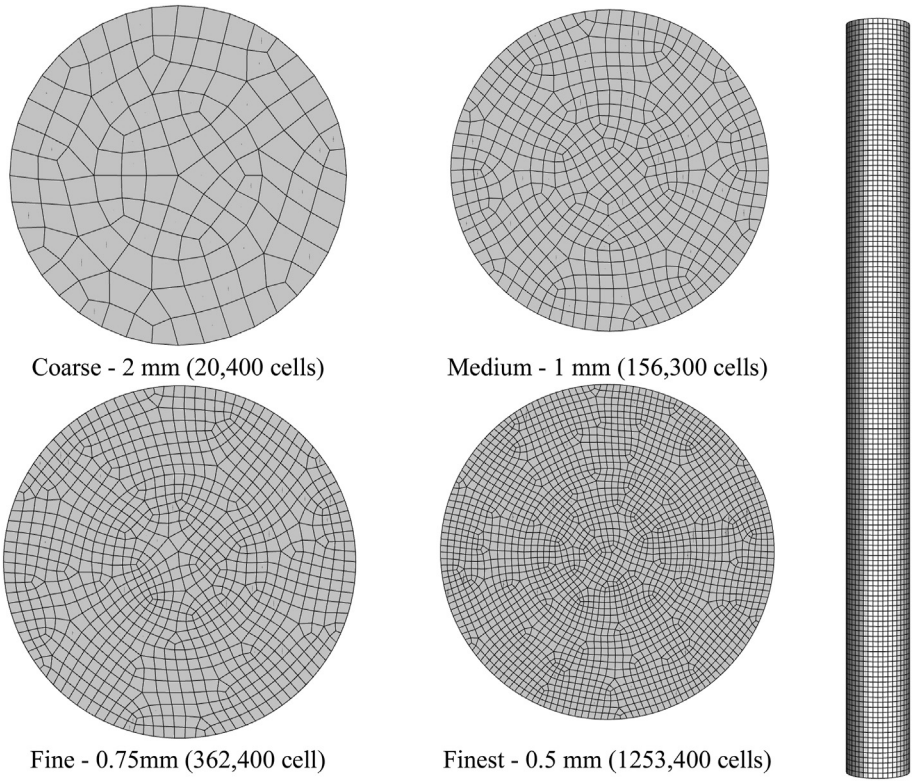

Fig. 2 – Membrane reactor grid resolution in the computational domain.

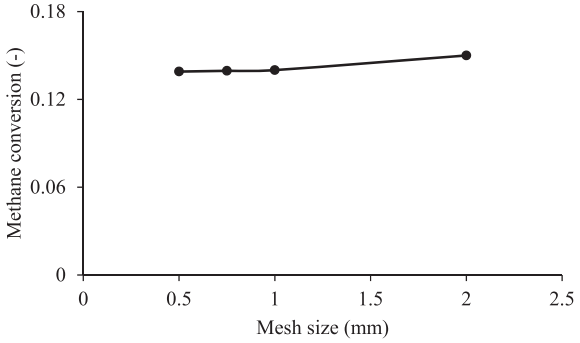

Fig. 3 – The simulated methane conversions for different grid resolutions.

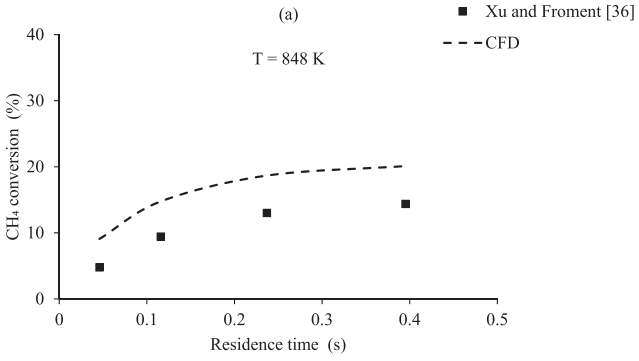

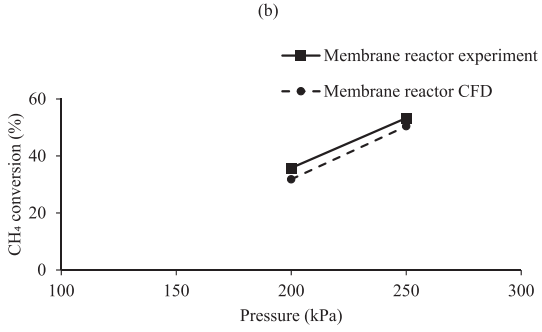

Fig. 4 – (a) MSR model validation at T – 848 K, P – 1000 kPa, S/C – 3 (b) Membrane reactor model validation at T – 773 K; GHSV – 837 h^{-1}; S/C – 3; P – 200, 250 kPa.

reported by Kim et al. [36]. Initially, MSR kinetic model was run at the same operating condition, after achieving a pseudo steady state hydrogen permeation model initiated. Model prediction for two different operating pressure shows the same methane conversion as we observed in the experiment, as shown in Fig. 4b. The resultant comparison between numerical and experimental results revealed the ability of the CFD to successfully predict the experiment data.

Effects of reaction temperature

The reaction temperature is a key parameter in the membrane reactor, and therefore the estimation of the performance of the reactor for different temperatures should be important for

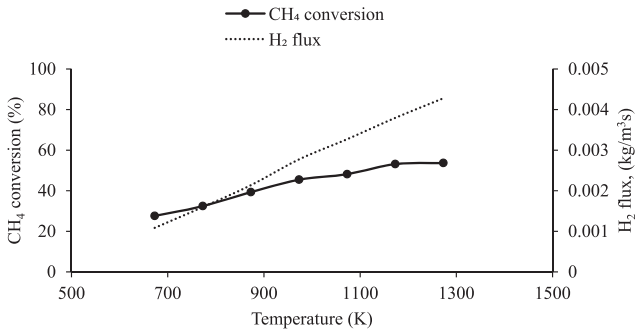

Fig. 5 – Effect of reaction temperature on methane conversion and hydrogen flux through the membrane. (GHSV – 837 h^{-1}; S/C – 3; P – 200 kPa).

practical application. To analyze the influence of reaction temperature, the simulation was performed under fixed GHSV of 837 h^{-1}, S/C ratio of 3 and retentate pressure of 200 kPa. The temperature was varied in the range of 673–1273 K. As shown in Fig. 5, methane conversion as a function of the temperature is constantly increased due to the endothermic characteristic as previously shown in the literature [43] Along with methane conversion, hydrogen permeation rate as a function of temperature was plotted in Fig.5. As the operating temperature increases the hydrogen separation rate is promoted Eq. (4). These predictions are in accordance with previous findings from literature [33,44].

For facilitating qualitative understanding, the model results of all three products (hydrogen, carbon dioxide, and carbon mono-oxide) obtained from the CFD simulation are visualized in Fig. 6. It seems that the CFD simulation was successfully able to capture the experimental trend of hydrogen, carbon dioxide, and carbon monoxide concentration as observed in the experiment [36]. Also, the hydrogen and carbon dioxide species concentration clearly increased with increasing in temperature. Indeed, the highest hydrogen species can be achieved by increasing the reforming temperature, because the steam reforming reaction is endothermic, favoring the high reaction temperatures. The quantitative comparison exhibited the obvious increase of the mean hydrogen mass fraction value with an increase in the reaction temperature. Overall performance of membrane reactor monotonically increases with temperature. However, the rate of methane conversion from 673 K to 973 K highest compared to temperature range of 1073 K–1273 K. Therefore, considering the Pd inorganic membrane performance with thermal stability the recommended operating temperature conditions between 673 K and 973 K.

Effect of GHSV

Another key operating parameter, the gas hourly space velocity (GHSV) was utilized to quantify the residence time of the reactant gases in a reactor during the operation. To find the potential application towards a large scale operation, the performance of MR was explored over a large range of GHSV. Fig. 7 shows the model results on the methane conversion according to the change of GHSV ranging from 837 h^{-1} to 10,000 h^{-1}, at the operating temperature and pressure of 773 K and 200 kPa respectively. From the modeling, with the given GHSV ranges, it seems that the methane conversion slightly decreased with an increase in GHSV. These predictions are consistence with other researcher findings [45]. However, increasing GHSV led to lower methane conversion, CH_4 conversion of 22% was still achievable by the membrane reformer. At higher GHSV

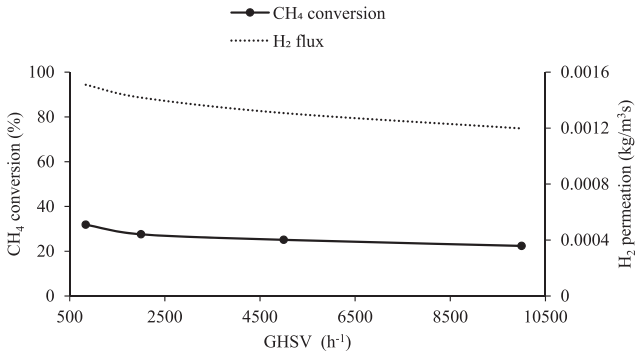

Fig. 7 – Effect of GHSV on methane conversion and hydrogen flux through the membrane. (GHSV – 837 h^{-1}; S/C – 3; P – 200 kPa).

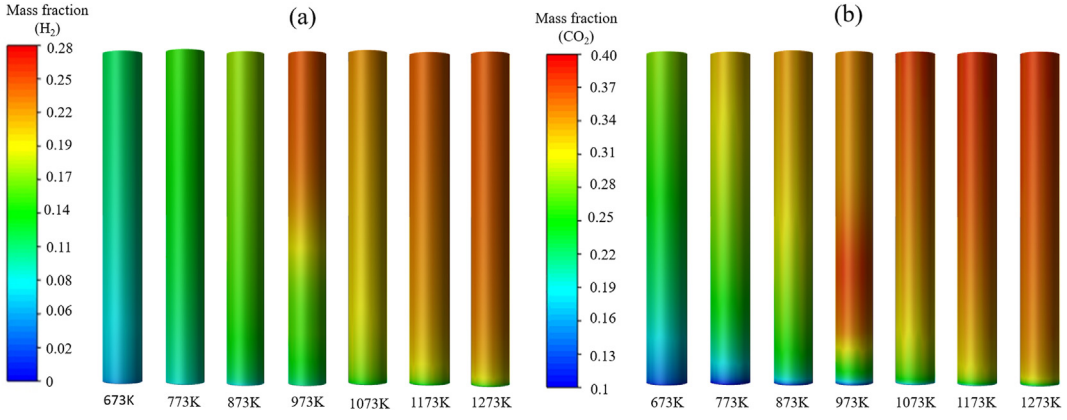

Fig. 6 – Contour plot of (a) H_2 species, (b) CO_2 species for different reaction temperature (GHSV – 837 h^{-1}; S/C – 3; P – 200 kPa).

result into decreasing the contact time with the membrane surface, which cause more decrease in H_2 permeation rate through the membrane as shown in Fig. 7. Similar observation was reported by Ma et al. [45]. However, in the meantime, a higher amount of CH_4 was feed into a reactor with higher GHSV. Thus, a very high feed rate of CH_4 gives reduction in the overall conversion rate.

In Fig. 8, it can be seen that at lower GHSV, a higher contact time in the reaction domain was favored. Specially, at low GHSV, helps higher hydrogen formation rate in the downstream direction. Thus, favor the higher hydrogen partial pressure which enhances the H_2 permeation and CO_2 adsorption rate helps effective shifting toward the products yield. Fig. 8b shows the temperature distribution profile for different GHSV (837, 2000, 5000, and 10000 h^{-1}). Here, the counterplot shows the temperature profile on the ZX plane. The simulation result shows two distinctive temperature profiles for retentate and permeate zone. The contour profile clearly explains that the mean temperature value is highest for 837 h^{-1} GHSV operating condition and lowest for 10000 h^{-1} GHSV operating condition. The above results highlight that for higher GHSV value methane conversion reached a plateau, thus considering the amount of reactant feed into membrane reactor require further detail parameter study in future work.

Effect of steam to carbon (S/C) ratio

After the analysis of the gas hourly space velocity, the reactant feed flow rate was fixed at a GHSV of 837 h^{-1}. Methane steam reforming in membrane reactor was tested under different steam to carbon ratio (S/C). Steam to methane (S/C) feed molar ratio is one of the key operational parameters that has large influence [46]. To understand the effect on the CH_4 conversion at the various steam-to-methane ratio simulation were carried out under fixed GHSV of 837 h^{-1}, 1073 k and retentate pressure of 200 kPa. The steam to methane ratio was varied in the range of 1–4. According to the Le Chatelier's principle, an increase in the reactant concentrations favored the forward reaction direction, therefore increase the methane conversion. Accordingly, the methane conversion increased from 45% to 49% for the corresponding increase in S/C ratios from 1 to 3, as shown in Fig. 9. The CFD model prediction shows good agreement with other published results [47,48]. However, in the presence of an excess of steam in the feed stream (S/C = 4), gives lower methane conversion, similar phenomenon has been previously observed in the literature [47]. Fig. 9 also reports hydrogen permeation rate for varying steam to methane ratio. As seen, the clear improvements achieved for hydrogen permeation as S/C increases from 1 to 3, whereas hydrogen permeation drops at S/C = 4. This outcome indicates that the excess steam diluted the mixture concentration and decreased hydrogen partial pressure difference between the reaction and the permeation zones [46]. The simulation results show that the influence of S/C ratio on the methane conversion and hydrogen permeation, it can be seen that the S/C of 3 is the optimal value.

Effect of sweep gas flow pattern

The membrane reactor performance in terms of methane conversion and hydrogen permeation for two different sweep flow configurations, namely co-current and counter-current was investigated. We evaluated the performance over range of sweep gas flow rate to attain optimum condition. By increasing the sweep gas flow rate CH_4 conversion and H_2

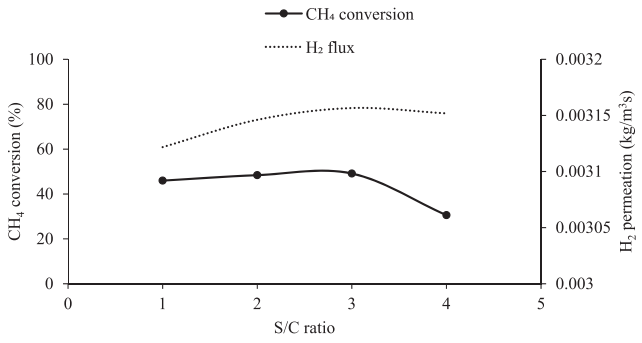

Fig. 9 – Effect of steam to carbon ratio on methane conversion and hydrogen flux through the membrane. (GHSV – 837 h^{-1}; P – 200 kPa).

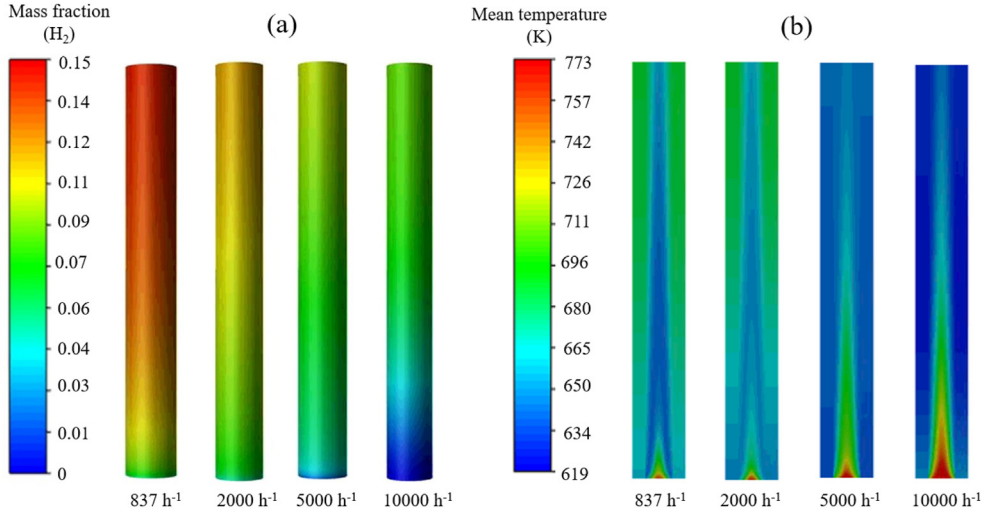

Fig. 8 – Contour plot of (a) H_2 species, (b) Z-X plan temperature profile for different GHSV (S/C – 3; P – 200 kPa).

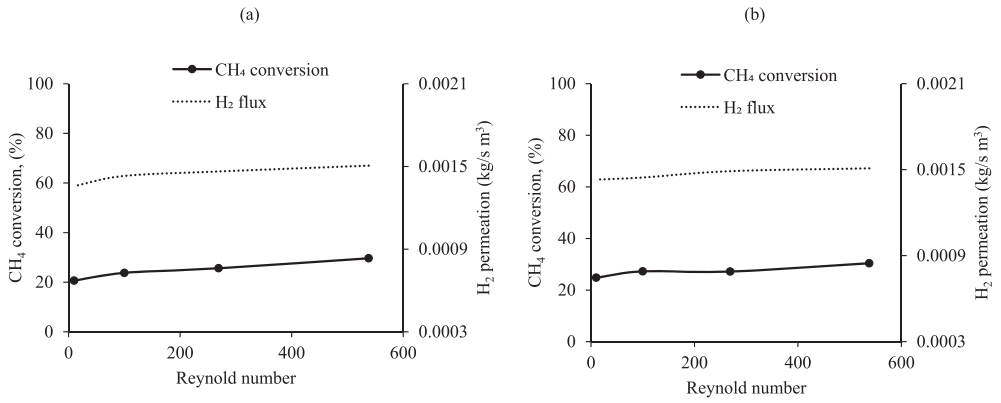

Fig. 10 – Effect of (a) co-current (b) counter current, sweep flow configuration on methane conversion and hydrogen flux through the membrane. (GHSV – 837 h^{-1}; S/C – 3; P – 200 kPa).

permeation increases for both counter-current and co-current mode as exhibited in Fig. 10. In particular, for the constant reactant feed rate, when the sweep gas flow rates increased, the average H_2 permeation across the membrane in co-current and counter-current flow configuration was enhanced by 7.8 and 12.6%, respectively. Similar increased permeation rate phenomenon was reported by Abdi et al. [49] and Gallucci et al. [50]. This implied that the sweep gas was able to effectively increase the H_2 permeation rate. As for the effect of the flow direction, H_2 separation from the counter-current mode was found to be better than that from the co-current once, this trend was consistent with the observations in the other studies [29]. Therefore, it is also found that H_2 separation positive influences resulting increased methane conversion with counter-current mode of operation. Increasing the flow rate of sweep gas diminished the difference of average H_2 permeation between the two current configurations. In particular, once the flow rate of sweep gas was higher, the difference became smaller. Such phenomena due to lessened concentration polarization on the membrane surface for a higher sweep gas flow rate. Overall performance between two flow configurations becomes smaller for a higher sweep gas flow rate. Such results clearly prove that continuous removal of hydrogen on the permeate zone enhances the overall hydrogen permeation. A sweep flow configuration sensitivity analysis suggest that counter-current modes give better performance in the whole range sweep gas flow rate. It is important to notice that at low sweep gas flow rate the methane conversion is high.

Conclusion

In the proposed study, the performance of a Palladium (Pd) membrane reactor for methane steam reforming (MSR) was demonstrated through a comprehensive three-dimensional (3D) computational fluid dynamic (CFD) analysis. For this purpose, retentate zone reforming reaction incorporate using the Xu and Forment kinetic model and hydrogen permeation via source and sink terms. Prior to detail operating sensitivity analysis, MSR reaction kinetic and permeation model were successfully validated with experimental data.

The developed model was then applied to investigate various operating conditions of the membrane reactor, and the results can be summarized as follows:

1) Simulation result proved that operating temperature is one of most influencing operation parameters. Temperature range of 673 K–973 K revealed optimal for balancing permeation and reaction performance.
2) Reduction in overall residence time resulted from an increase in the gas flow rate, leading to a decrease in H_2 permeation. Hence, methane conversion and H_2 separation performances higher at lower GHSV.
3) With increasing the steam to methane (S/C) ratios from 1 to 3, methane conversion increased from 45% to 49%, except for the ratio of 4.
4) Simulation results predicts increase in the CH_4 conversion and H_2 permeation with increase in sweep gas flow rate. Also, we observe that the permeation and reaction performance with counter-current configuration is better than the co-current configuration.

Declaration of competing interest

The authors declare that they have no known competing financial interests or personal relationships that could have appeared to influence the work reported in this paper.

Acknowledgement

This work was supported by the Korea Institute of Energy Technology Evaluation and Planning (KETEP) granted financial resource from the Ministry of Trade, Industry & Energy, Republic of Korea (No. 20183010032380) also this research was supported by the Hydrogen Energy Innovation Technology Development Program of the National Research Foundation of

Korea funded by the Korean government (Ministry of Science and ICT (MSIT)) (NRF-2019M3E6A1064290).

Appendix A

Continuity equation and Momentum conservation equation

Continuity equation:

$$\nabla \cdot (\rho \vec{u}) = 0 \quad \text{(a)}$$

Momentum equation:

$$\nabla \cdot (\rho \vec{u}\vec{u}) = -\nabla p + \nabla \cdot \bar{\bar{\tau}} + \rho g + F \quad \text{(b)}$$

$$F = -\left(\frac{\mu_e}{\alpha}\vec{u} + C_0 \frac{1}{2}\rho|\vec{u}|\vec{u}\right), \mu_e = \mu(1 + 2.5(1-\gamma))$$

Energy Equation:

$$\nabla \cdot (\vec{u}(\rho E + p)) = \nabla \cdot \left(k_{eff}\nabla T + \sum h_i \overrightarrow{J_i} + (\vec{u} \cdot \overline{\bar{\tau}_{eff}})\right) + \sum h_i R_i + \nabla \cdot \overrightarrow{q_{rad}} \quad \text{(c)}$$

Species equation:

$$\nabla \cdot (\rho \vec{u} Y_i) = \nabla \cdot \vec{J_i} + R_i \quad \text{(d)}$$

REFERENCES

[1] Yan Y, Zhien Z, Zhang Li, Wang X, Liu K, Yang Z. Investigation of autothermal reforming of methane for hydrogen production in a spiral multi-cylinder micro-reactor used for mobile fuel cell. Int J Hydrogen Energy 2015;40:1886–93.

[2] Tran A, Aguirre A, Crose M, Durand H, Christofide PD. Temperature balancing in steam methane reforming furnace via an integrated CFD/data-based optimization approach. Comput Chem Eng 2017;104:185–200.

[3] Celik D, Yildiz M. Investigation of hydrogen production methods in accordance with green chemistry principles. Int J Hydrogen Energy 2017;42:23395–401.

[4] Upadhyay M, Lee S, Jung S, Choi Y, Moon S, Lim H. Systematic assessment of the anode flow field hydrodynamics in a new circular PEM water electrolyser. Int J Hydrogen Energy 2020;45:20765–75.

[5] Ewan BCR, Allen RWK. A figure of merit assessment of the routes to hydrogen. Int J Hydrogen Energy 2005;30:809–19.

[6] Ardaneh M, Abolhasani M, Esmaeili M. CFD modeling of two-stage H2 recovery process from ammonia purge stream by industrial hollow fiber membrane modules. Int J Hydrogen Energy 2019;44:4851–67.

[7] Saedi S, Madaeni SS, Shamsabadi AA. PDMS coated asymmetric PES membrane for natural gas sweetening: effect of preparation and operating parameters on performance. Can J Chem Eng 2014;92:892–904.

[8] Kargari A, Shamsabadi AA, Babaheidari MB. Influence of coating conditions on the H2 separation performance from H2/CH4 gas mixtures by the PDMS/PEI composite membrane. Int J Hydrogen Energy 2014;39:6588–97.

[9] Montaleone D, Mercadelli E, Escolástico S, Gondolini A, Serra JM, Sanson A. All-ceramic asymmetric membranes with superior hydrogen permeation. J Mater Chem 2018;6:15718–27.

[10] Zhu Z, Sun W, Wang Z, Cao J, Dong Y, Liu W. A high stability Ni–$La_{0.5}Ce_{0.5}O_{2-\delta}$ asymmetrical metal-ceramic membrane for hydrogen separation and generation. J Power Sources 2015;281:417–24.

[11] Castro-Muñoz R, Martin-Gil V, Ahmad MZ, Fíla V. Matrimid® 5218 in preparation of membranes for gas separation: current state-of-the-art. Chem Eng Commun 2018;205:161–96.

[12] Livshits AI. The hydrogen transport through the metal alloy membranes with a spatial variation of the alloy composition: potential diffusion and enhanced permeation. Int J Hydrogen Energy 2017;42:13111–9.

[13] Nayebossadri S, Speight JD, Book D. Hydrogen separation from blended natural gas and hydrogen by Pd-based membranes. Int J Hydrogen Energy 2019;44:29092–9.

[14] Gallucci F, Pacheco Tanaka DA, Medrano JA, Viviente Sole JL. Book chapter: membrane reactors using metallic membranes. Current Trends and Future Developments on (Bio-) Membranes 2020:235–60.

[15] Li L, Ma G, Pan Z, Zhang N, Zhang Z. Research progress in gas separation using hollow fiber membrane contactors. Membranes 2020;10:380–400.

[16] Iulianelli A, Manzolini G, De Falco M, Campanari S, Longo T, Liguori S, Basile A. H_2 production by low pressure methane steam reforming in a Pd–Ag membrane reactor over a Ni-based catalyst: experimental and modeling. Int J Hydrogen Energy 2010;35:11514–24.

[17] Kim CH, Han JY, Lim H, Lee KY, Ryi SK. Methane steam reforming using a membrane reactor equipped with a Pd-based composite membrane for effective hydrogen production. Int J Hydrogen Energy 2018;43:5863–72.

[18] Nayebossadri S, Speight JD, Book D. Hydrogen separation from blended natural gas and hydrogen by Pd-based membranes. Int J Hydrogen Energy 2019;44:29092–9.

[19] Rahimpour MR, Samimi F, Babapoor A, Tohidian T, Mohebi S. Palladium membranes applications in reaction systems for hydrogen separation and purification: a review. Chem Eng Process: Process Intensification 2017;121:24–49.

[20] Alique D, Martinez-Diaz D, Sanz R, Calles JA. Review of supported Pd-based membranes preparation by electroless plating for ultra-pure hydrogen production. Membranes 2018;8:5.

[21] Castro-Dominguez B, Mardilovich IP, Ma LC, Ma R, Dixon AG, Kazantzis NK, Ma YH. Integration of methane steam reforming and water gas shift reaction in a Pd/Au/Pd-based catalytic membrane reactor for process intensification. Membranes 2016;6:44.

[22] Meng L, Yu X, Niimi T, Nagasawa H, Kanezashi M, Yoshioka T, Tsuru T. Methylcyclohexane dehydrogenation for hydrogen production via a bimodal catalytic membrane reactor. AIChE J 2015;61:1628–38.

[23] Li G, Yada K, Kanezashi M, Yoshioka T, Tsuru T. Methylcyclohexane dehydrogenation in catalytic membrane reactors for efficient hydrogen production. Ind Eng Chem Res 2013;52:13325–32.

[24] Benguerba Y, Amer J, Ernst B. CFD modeling of the H_2/N_2 separation with a nickel/α-alumina microporous membrane. Chem Eng Sci 2015;123:527–35.

[25] Benguerba Y, Dumas C, Ernst B. Modelling of the membrane permeability effect on the H_2 production using CFD method. Int J Chem React Eng 2014;1 [open-issue)].

[26] Ghohe FM, Hormozi F. A numerical investigation on H_2 separation by a conical palladium membrane. Int J Hydrogen Energy 2019;44:10653–65.

[27] Chen WH, Kuo PC, Lin YL. Evolutionary computation for maximizing CO_2 and H_2 separation in multiple-tube palladium-membrane systems. Appl Energy 2019;235:299–310.

[28] Ben-Mansour R, Abuelyamen A, Habib MA. CFD modeling of hydrogen separation through Pd-based membrane. Int J Hydrogen Energy 2020;45:23006–19.
[29] Chen WH, Syu WZ, Hung CI, Lin YL, Yang CC. A numerical approach of conjugate hydrogen permeation and polarization in a Pd membrane tube. Int J Hydrogen Energy 2012;37:12666–79.
[30] Coroneo M, Montante G, Catalano J, Paglianti A. Modelling the effect of operating conditions on hydrodynamics and mass transfer in a Pd–Ag membrane module for H2 purification. J Membr Sci 2009;343:34–41.
[31] Said SA, Simakov DS, Waseeuddin M, Román-Leshkov Y. Solar molten salt heated membrane reformer for natural gas upgrading and hydrogen generation: a CFD model. Sol Energy 2016;124:163–76.
[32] Said SA, Simakov DS, Mokheimer EM, Habib MA, Ahmed S, Waseeuddin M, Román-Leshkov Y. Computational fluid dynamics study of hydrogen generation by low temperature methane reforming in a membrane reactor. Int J Hydrogen Energy 2015;40:3158–69.
[33] Sanusi YS, Mokheimer EM. Performance analysis of a membrane-based reformer-combustor reactor for hydrogen generation. Int J Energy Res 2019;43:189–203.
[34] Xuan J, Leung DY, Leung MK, Ni M, Wang H. Chemical and transport behaviors in a microfluidic reformer with catalytic-support membrane for efficient hydrogen production and purification. Int J Hydrogen Energy 2012;37:2614–22.
[35] Tahmasbi D, Hossainpour S, Babaluo AA, Rezakazemi M, Souq SSMN, Younas M. Hydrogen separation from synthesis gas using silica membrane: CFD simulation. Int J Hydrogen Energy 2020;45:19381–90.
[36] Kim CH, Han JY, Lim H, Kim DW, Ryi SK. Methane steam reforming in a membrane reactor using high-permeable and low-selective Pd-Ru membrane. Kor J Chem Eng 2017;34:1260–5.
[37] Xu J, Froment GF. Methane steam reforming, methanation and water-gas shift: I. Intrinsic kinetics. AIChE J 1989;35:88–96.
[38] Xu J, Froment GF. Methane steam reforming: II. Diffusional limitations and reactor simulation. AIChE J 1989;35:97–103.
[39] Oliveira EL, Grande CA, Rodrigues AE. Steam methane reforming in a Ni/Al2O3 catalyst: kinetics and diffusional limitations in extrudates. Can J Chem Eng 2009;87:945–56.
[40] Lao L, Aguirre A, Tran A, Wu Z, Durand H, Christofides PD. CFD modeling and control of a steam methane reforming reactor. Chem Eng Sci 2016;148:78–92.
[41] Chapman S, Cowling TG, Burnett D. The mathematical theory of non-uniform gases: an account of the kinetic theory of viscosity, thermal conduction and diffusion in gases. Cambridge university press; 1990.
[42] Gallucci F, De Falco M, Tosti S, Marrelli L, Basile A. Ethanol steam reforming in a dense Pd–Ag membrane reactor: a modelling work. Comparison with the traditional system. Int J Hydrogen Energy 2008;33:644–51.
[43] Pashchenko D. Experimental study of methane reforming with products of complete methane combustion in a reformer filled with a nickel-based catalyst. Energy Convers Manag 2019;183:159–66.
[44] Ma R, Castro-Dominguez B, Mardilovich IP, Dixon AG, Ma YH. Experimental and simulation studies of the production of renewable hydrogen through ethanol steam reforming in a large-scale catalytic membrane reactor. Chem Eng J 2016;303:302–13.
[45] Nam SW, Yoon SP, Ha HY, Hong SA, Maganyuk AP. Methane steam reforming in a Pd–Ru membrane reactor. Kor J Chem Eng 2000;17:288–96.
[46] Amiri TY, Ghasemzageh K, Iulianelli A. Membrane reactors for sustainable hydrogen production through steam reforming of hydrocarbons: a review. Chemical Engineering and Processing - Process Intensification 2020;157:108148.
[47] Chibane L, Djellouli B. Methane steam reforming reaction behaviour in a packed bed membrane reactor. Int J Chem Eng Appl 2011;2:147–56.
[48] Roses L, Campanari S, Manzolini G. 14 - computational fluid dynamics (CFD) analysis of membrane reactors: simulation of a palladium-based membrane reactor in fuel cell micro-cogenerator system. Handbook of membrane reactors, vol. 1. Woodhead Publishing; 2013. p. 496–531. 1.
[49] Abdi H, Pourmahmoud N, Soltan J. A novel CFD simulation of H_2 separation by Pd-based helical and straight membrane tubes. Kor J Chem Eng 2020;37:2041–53.
[50] Gallucci F, De Falco M, Tosti S, Marrelli L, Basile A. Co-current and counter-current configurations for ethanol steam reforming in a dense Pd–Ag membrane reactor. Int J Hydrogen Energy 2008;33:6165–71.

Nomenclature

T: Temperature (K or °C)
P: Pressure (kPa)
p_i: Partial pressure of species i, bar
D: Diameter, mm
L: Length, mm
r_n: nth chemical reaction rate (kmol/m^3/s)
k_n: Kinetic parameter of reaction nth (Table 3)
K_{en}: Equilibrium constant (Table 3)
K_i: Adsorption constants of species i (Table 3)
R: Gas constant (8.314×10^3 J/kmol/K)
c_p: Specific heat capacity (J/kg/K)
M_w: Molecular weight (kg/kmol)
A_c: Area of membrane boundary cell (m^2)
V_c: Volume of membrane boundary cell (m^3)
P_e: Pre-exponential factor (mol/m2/s/Pa$^{0.5}$)
l: Membrane thicknesses (m)
P_{r,H_2}: Partial pressure of hydrogen in retentate side (Pa)
P_{p,H_2}: Partial pressure of hydrogen in permeate side (Pa)
E_a: Activation energy (kJ/mol)

Greek Letters

γ: Thermal conductivity (W/m/K)
μ_i: Viscosity of the ith species (kg/m/s)
β: Membrane effectiveness factor (–)

Abbreviation

GHSV: Gas hourly space velocity
CFD: Computational fluid dynamics